6

Physical realizations

We are still at the very beginnings of physical implementations of quantum computers. The devices listed below have been used successfully to entangle two qubits (at most!), except for NMR which has gone up to 7 qubits. It is still premature to try to predict which device will prove most effective for building a quantum computer capable of dealing with several hundred qubits (if such a computer someday exists); perhaps it will be something new, not on this list at all. In any case, it would be as foolish to predict that such a computer will not be available by 2050 as to predict the contrary. [1]

The storage and processing of quantum information requires physical systems possessing the following properties (di Vincenzo criteria):

(i) they must be scalable, that is, capable of being extended to a sufficient number of qubits, with well defined qubits;
(ii) they must have qubits which can be initialized in the state $|0\rangle$;
(iii) they must have qubits which are carried by physical states of sufficiently long lifetime, so as to ensure that the quantum states remain coherent throughout the calculation;
(iv) they must possess a set of universal quantum gates: unitary transformations on individual qubits and a cNOT gate, which are obtained by controlled manipulations;
(v) there must be an efficient procedure for measuring the state of the qubits at the end of the calculation (*readout* of the results).

The Enemy Number One of a quantum computer is interaction with the environment leading, as we have seen in Section 4.4, to the phenomenon of decoherence, a consequence of which is the loss of the phase in the linear superposition of qubits. The calculations must be performed in a time less than the decoherence

[1] We note that the time scale here is similar to that foreseen for obtaining energy from fusion, a first step in this direction being the ITER project.

https://doi.org/10.1017/CBO9780511755361.008

time τ_D. If an elementary operation (logic gate) on a qubit takes a time τ_{op}, the figure of merit for a quantum computer is the ratio

$$n_{op} = \frac{\tau_D}{\tau_{op}}.$$

This is the maximum number of operations that the quantum computer can perform. The devices imagined up to now include the following (this list is not exhaustive):

- a photonic quantum computer based on the nonlinear Kerr effect;
- optical resonant cavities;
- microwave resonant cavities;
- ion traps;
- nuclear magnetic resonance;
- superconducting circuits with Josephson junctions;
- quantum dots;
- atoms of a Bose–Einstein condensate trapped in an optical lattice.

In this chapter we shall limit ourselves to four types of device: NMR (Section 6.1), trapped ions (Section 6.2), superconducting qubits (Section 6.3), and quantum dots (Section 6.4). The necessary background for understanding NMR quantum computers has been given in Section 3.4. However, Sections 6.2 to 6.4 require a more advanced knowledge of physics than has been assumed up to now in this book, even though we restrict ourselves to schematic descriptions. The reader can proceed directly to Chapter 7 (quantum information), which is completely independent of the present chapter.

6.1 NMR as a quantum computer

The record in the number of qubits was set in 2001 by a quantum computer using NMR. In spite of this record, NMR is certainly not a solution with a future, owing to problems which we shall discuss later on. As a preliminary, let us reformulate the results of Section 3.3 using a more abstract but also more general formalism, which will allow us in particular to treat easily the case of two coupled spins. The Hamiltonian (3.24) can be written as

$$\hat{H}(t) = \hat{H}_0 + \hat{H}_1(t) = -\frac{\hbar}{2}\omega_0\sigma_z - \frac{\hbar}{2}\omega_1\left(\sigma_+ e^{i\omega t} + \sigma_- e^{-i\omega t}\right) \tag{6.1}$$

with $\sigma_\pm = (\sigma_x \pm i\sigma_y)/2$:

$$\sigma_+ = \begin{pmatrix} 0 & 1 \\ 0 & 0 \end{pmatrix}, \qquad \sigma_- = \sigma_+^\dagger = \begin{pmatrix} 0 & 0 \\ 1 & 0 \end{pmatrix}.$$

https://doi.org/10.1017/CBO9780511755361.008

To study the evolution of the state vector $|\varphi(t)\rangle$ we define the state vector $|\tilde{\varphi}(t)\rangle$ in the "rotating reference frame" as

$$|\tilde{\varphi}(t)\rangle = \exp\left[-\frac{\mathrm{i}\omega\sigma_z t}{2}\right]|\varphi(t)\rangle. \tag{6.2}$$

To interpret this reference frame physically, we note that $|\tilde{\varphi}(t)\rangle$ is independent of time for $\omega = \omega_0$ and $\omega_1 = 0$:

$$|\tilde{\varphi}(t)\rangle = |\tilde{\varphi}(t=0)\rangle \qquad \omega = \omega_0, \qquad \omega_1 = 0$$

because

$$|\varphi(t)\rangle = \mathrm{e}^{-\mathrm{i}\hat{H}_0 t/\hbar}|\varphi(0)\rangle = \mathrm{e}^{\mathrm{i}\omega\sigma_z t/2}|\varphi(0)\rangle \qquad \text{if} \qquad \omega = \omega_0. \tag{6.3}$$

This tells us that the spin remains at rest in the rotating reference frame, and so the expectation value $\langle\tilde{\varphi}(t)|\vec{\sigma}|\tilde{\varphi}(t)\rangle$ of $\vec{\sigma}$ is independent of time, while in the laboratory frame this expectation value rotates with angular velocity ω_0. In general, when $\omega \neq \omega_0$ the spin rotates in the frame (6.2) with angular velocity $(\omega_0 - \omega)$. We can easily obtain the evolution equation of $|\tilde{\varphi}(t)\rangle$ when $\omega_1 \neq 0$:

$$\mathrm{i}\hbar\frac{\mathrm{d}|\tilde{\varphi}\rangle}{\mathrm{d}t} = \left(\frac{\hbar}{2}\delta\sigma_z - \frac{\hbar}{2}\omega_1\sigma_x\right)|\tilde{\varphi}(t)\rangle = \tilde{H}|\tilde{\varphi}(t)\rangle. \tag{6.4}$$

We recall that $\delta = \omega - \omega_0$ is the detuning defined in Fig. 3.4. The Hamiltonian $\tilde{H}$ has become independent of time in the rotating frame! In obtaining (6.4) we have used

$$\tilde{H}(t) = \frac{\hbar}{2}\omega\sigma_z + \mathrm{e}^{-\mathrm{i}\omega\sigma_z t/2}\,\hat{H}(t)\,\mathrm{e}^{\mathrm{i}\omega\sigma_z t/2}$$

and [2]

$$\tilde{\sigma}_\pm(t) = \mathrm{e}^{-\mathrm{i}\omega\sigma_z t/2}\,\sigma_\pm\,\mathrm{e}^{\mathrm{i}\omega\sigma_z t/2} = \mathrm{e}^{\mp\mathrm{i}\omega t}\sigma_\pm. \tag{6.5}$$

Now we can give a geometrical interpretation of the effect of the radiofrequency field in the rotating frame. To simplify matters let assume that $\omega = \omega_0$ and leave the general case to Exercise 6.5.1. Then

$$\mathrm{e}^{-\mathrm{i}\tilde{H}t/\hbar} = \mathrm{e}^{\mathrm{i}\omega_1\sigma_x t/2} = \cos\frac{\omega_1 t}{2} + \mathrm{i}\sigma_x\,\sin\frac{\omega_1 t}{2}. \tag{6.6}$$

Since the operator [3] which rotates the spin by an angle θ about Ox is $R_x(\theta) = \exp(-\mathrm{i}\theta\sigma_x/2)$, we see that $\exp(\mathrm{i}\omega_1 t\sigma_x/2)$ is the operator which rotates by an

[2] The simplest way to find (6.5) is to note that $\tilde{\sigma}_\pm(t)$ satisfies the differential equation

$$\frac{\mathrm{d}\tilde{\sigma}_\pm(t)}{\mathrm{d}t} = -\frac{\mathrm{i}\omega}{2}\,\mathrm{e}^{-\mathrm{i}\omega\sigma_z t/2}\,[\sigma_z, \sigma_\pm]\,\mathrm{e}^{\mathrm{i}\omega\sigma_z t/2} = \mp\mathrm{i}\omega\tilde{\sigma}_\pm(t)$$

because $[\sigma_z, \sigma_\pm] = \pm 2\sigma_\pm$.

[3] We refer the reader to Exercise 3.5.1.

angle $\theta = -\omega_1 t$ about Ox. The spin can be made to rotate by a given angle by adjusting the duration t of the radiofrequency pulse. In particular, a $\pi/2$ pulse (Section 3.3) of duration $\omega_1 t/2 = \pi/4$ rotates the spin by $\pi/2$ about Ox: if the spin is initially along Oz, then this rotation aligns it with Oy.

The advantage of the preceding formalism is that it permits a convenient treatment of the case of two coupled spins, which we shall now study. In order to avoid a proliferation of indices, we use (X, Y, Z) to denote the Pauli matrices:

$$X \equiv \sigma_x, \qquad Y \equiv \sigma_y, \qquad Z \equiv \sigma_z. \tag{6.7}$$

Let us consider two spins 1/2 attached to the *same* molecule,[4] for example, the first spin (1) carried by a proton and the second (2) carried by a ^{13}C nucleus. These two spins have different magnetic moments and therefore different resonance frequencies $\omega_0^{(1)}$ and $\omega_0^{(2)}$ and different Rabi frequencies $\omega_1^{(1)}$ and $\omega_1^{(2)}$. If the two spins are carried by identical nuclei, it is the chemical shift which causes the resonance frequencies to be different, but the difference will of course be very small in this case, $\sim 10^{-5}$ in relative value. The spins are coupled by an interaction[5] of the type $\hbar J Z_1 Z_2$ (more correctly, $\hbar J Z_1 \otimes Z_2$, but we shall frequently omit the tensor product notation: $Z_1 Z_2 \equiv Z_1 \otimes Z_2$, $Z_2 \equiv I_1 \otimes Z_2$, and so on). The Hamiltonian $\hat{H}_{12}(t)$ of the set of two spins is then obtained by generalizing (6.1):

$$\begin{aligned}\hat{H}_{12}(t) = &-\frac{\hbar}{2}\omega_0^{(1)} Z_1 - \frac{\hbar}{2}\omega_0^{(2)} Z_2 - \frac{\hbar}{2}\omega_1^{(1)}\left(\sigma_{1+}\,\mathrm{e}^{\mathrm{i}\omega^{(1)}t} + \sigma_{1-}\,\mathrm{e}^{-\mathrm{i}\omega^{(1)}t}\right) \\ &- \frac{\hbar}{2}\left(\omega_1^{(2)}\sigma_{2+}\,\mathrm{e}^{\mathrm{i}\omega^{(2)}t} + \sigma_{2-}\,\mathrm{e}^{-\mathrm{i}\omega^{(2)}t}\right) + \hbar J Z_1 Z_2\end{aligned} \tag{6.8}$$

with $\sigma_{i\pm} = (X_i \pm \mathrm{i} Y_i)/2$. Since the resonance frequencies are different, the fields applied to the two spins will have different frequencies, adjusted to be in quasi-resonance with each spin:

$$|\delta^{(1)}| = |\omega^{(1)} - \omega_0^{(1)}| \ll \omega_1^{(1)}, \qquad |\delta^{(2)}| = |\omega^{(2)} - \omega_0^{(2)}| \ll \omega_1^{(2)}. \tag{6.9}$$

In the rotating frame the state vector $|\tilde{\varphi}_1(t) \otimes \tilde{\varphi}_2(t)\rangle$ of the system of two spins is given by the generalization of (6.2):

$$|\tilde{\varphi}_1(t) \otimes \tilde{\varphi}_2(t)\rangle = \exp\left[-\frac{\mathrm{i}\omega^{(1)} Z_1 t}{2}\right] \exp\left[-\frac{\mathrm{i}\omega^{(2)} Z_2 t}{2}\right] |\varphi_1(t) \otimes \varphi_2(t)\rangle. \tag{6.10}$$

In this reference frame the Hamiltonian is as before independent of time:

$$\tilde{H} = \frac{\hbar}{2}\delta_1 Z_1 + \frac{\hbar}{2}\delta_2 Z_2 - \frac{\hbar}{2}\omega_1^{(1)} X_1 - \frac{\hbar}{2}\omega_1^{(2)} X_2 + \hbar J Z_1 Z_2, \tag{6.11}$$

[4] The molecules are diluted in a solvent, and the interactions between the "active" molecules, that is, those carrying the qubits, are negligible.

[5] This interaction is indirect and is not due to an interaction between the magnetic moments. It is transmitted by the electrons involved in the same chemical bond.

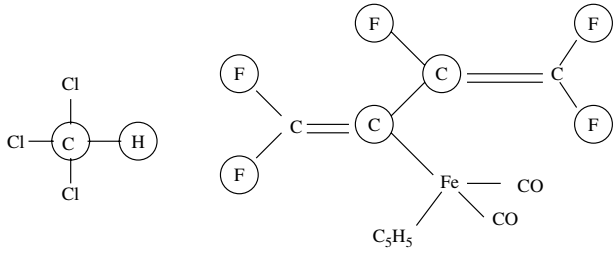

Figure 6.1 Two molecules used for quantum computing; the atoms carrying the active qubits are circled. (a) Chloroform, 2 qubits; (b) a perfluorobutadienyl iron complex, 7 qubits.

where we have used the fact that Z_1Z_2 commutes with Z_1 and Z_2. In what follows it will be important to bear in mind that the condition $|J| \ll \omega_1^{(1)}, \omega_1^{(2)}$ is always satisfied in practice. Two examples of molecules which have been used successfully are given in Fig. 6.1.

Let us now consider the quantum logic gates. The qubits are of course spins 1/2; for the moment we shall ignore the fact that the qubits are in a complex environment, and proceed as though we were dealing with individual qubits. The manipulation of qubits one by one corresponding to one-qubit logic gates is obvious: it is sufficient to apply a radiofrequency field for a suitable time interval, where the frequency is close to the resonance frequency $\omega_0^{(i)}$ of the qubit (i) which we wish to manipulate.

The cNOT gate is realized using the interaction $JZ_1 \otimes Z_2$ between the two qubits. As we have seen, it is impossible to realize a cNOT gate by manipulating individual qubits. NMR differs from other quantum computer devices in that the interaction between qubits is not introduced externally, but is *internal to the system*. The interaction $JZ_1 \otimes Z_2$ between the spins is always present, and the problem is to suppress its effects when we want certain qubits not to evolve. We shall use the fact that the typical time needed for the $JZ_1 \otimes Z_2$ term to perform a rotation of two qubits (several milliseconds) is about two orders of magnitude larger than the time needed for the radiofrequency field to rotate an individual qubit (about ten microseconds). We can immediately calculate the evolution operator $\exp(-\mathrm{i}tJZ_1 \otimes Z_2)$ using

$$(Z_1 \otimes Z_2)(Z_1 \otimes Z_2) = Z_1^2 \otimes Z_2^2 = I_{12}.$$

We then find

$$\exp(-\mathrm{i}Jt\, Z_1 \otimes Z_2) = I_{12} \cos Jt - \mathrm{i}(Z_1 \otimes Z_2) \sin Jt. \tag{6.12}$$

The following realization of a cNOT gate uses the operators performing $\pi/2$ rotations applied to individual qubits. The operators which rotate by an angle $\pi/2$ about Ox, Oy, and Oz, that is, $R_x(\pi/2)$, $R_y(\pi/2)$, and $R_z(\pi/2)$, are obtained using the fact that $\exp(-\mathrm{i}\theta\vec{\sigma}\cdot\hat{n}/2)$ is the operator for a rotation $R_{\hat{n}}(\theta)$ by an angle θ about the $\hat{n}$ axis (Exercise 3.5.1). We then have

$$R_x(\pi/2) = \frac{1}{\sqrt{2}}(I - \mathrm{i}X), \qquad R_y(\pi/2) = \frac{1}{\sqrt{2}}(I - \mathrm{i}Y), \qquad R_z(\pi/2) = \frac{1}{\sqrt{2}}(I - \mathrm{i}Z). \tag{6.13}$$

We define the operator $X_{12}(t)$ acting on the ensemble of two spins

$$X_{12}(t) = \exp[\mathrm{i}Jt(Z_1 \otimes Z_2)]\, R_z^{(1)}(\pi/2)\, R_z^{(2)}(\pi/2)$$

during a time t such that $Jt = \pi/4$:

$$\exp[\mathrm{i}\pi(Z_1 \otimes Z_2)/4] = \frac{1}{\sqrt{2}}(1 + \mathrm{i}Z_1 \otimes Z_2).$$

Now we have

$$X_{12}\left(\frac{\pi}{4J}\right) = \left(\frac{1}{\sqrt{2}}\right)^3 (I_{12} + \mathrm{i}Z_1 \otimes Z_2)(I_{12} - \mathrm{i}Z_1 \otimes I_2)(I_{12} - \mathrm{i}I_1 \otimes Z_2).$$

The multiplication can be done immediately, giving

$$X_{12}\left(\frac{\pi}{4J}\right) = \frac{1-\mathrm{i}}{\sqrt{2}}(1 + Z_1 \otimes I_2 + I_1 \otimes Z_2 - Z_1 \otimes Z_2) = \frac{1-\mathrm{i}}{\sqrt{2}}\,\mathrm{cZ}, \tag{6.14}$$

where the cZ (control-Z) gate is

$$\mathrm{cZ} = \begin{pmatrix} 1 & 0 & 0 & 0 \\ 0 & 1 & 0 & 0 \\ 0 & 0 & 1 & 0 \\ 0 & 0 & 0 & -1 \end{pmatrix} = \begin{pmatrix} I & 0 \\ 0 & \sigma_z \end{pmatrix}.$$

To go from the cZ gate to the cNOT = cX gate, it is sufficient to sandwich the former between two Hadamard gates acting on qubit 2:

$$\mathrm{cNOT} = (I_1 \otimes H_2)\,\mathrm{cZ}(I_1 \otimes H_2). \tag{6.15}$$

In fact,

$$\begin{pmatrix} H & 0 \\ 0 & H \end{pmatrix}\begin{pmatrix} I & 0 \\ 0 & \sigma_z \end{pmatrix}\begin{pmatrix} H & 0 \\ 0 & H \end{pmatrix} = \begin{pmatrix} H^2 & 0 \\ 0 & H\sigma_z H \end{pmatrix} = \begin{pmatrix} I & 0 \\ 0 & \sigma_x \end{pmatrix}.$$

The Hadamard gate corresponds to a rotation of π about the axis $(1/\sqrt{2}, 0, 1/\sqrt{2})$:

$$\exp\left(\frac{-\mathrm{i}\pi(\sigma_x + \sigma_z)}{2\sqrt{2}}\right) = -\mathrm{i}H,$$

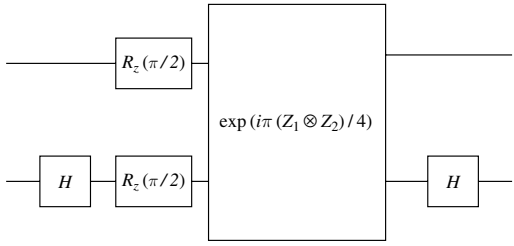

Figure 6.2 NMR construction of a cNOT gate. The diagrams are read from left to right, and the operator products are taken from right to left.

but in practice rotations about Ox or Oy are always used. The time needed for the rotations $R_z(\pi/2)$ or H (about ten microseconds) is negligible compared to the time needed for the evolution due to the term $JZ_1 \otimes Z_2$ (several milliseconds), and this evolution is negligible during the time needed for the individual rotations. The logic circuit corresponding to the operations (6.14) and (6.15) is shown in Fig. 6.2.

However, during the several milliseconds needed to realize the gate, the other qubits continue to evolve according to the various terms in the Hamiltonian. The NMR signal is not produced by a single spin, but by an ensemble of spins ($\sim 10^{18}$ of them, the minimum number needed to obtain a measurable signal). The nonuniformities of the field $\vec{B}_0$ and other random phenomena cause the qubits carried by different molecules to evolve differently, and so the signal will become fuzzy. This is why it is necessary to resort to the technique of *refocusing* (spin echo), a basic tool used in modern NMR and MRI. We shall explain it here for the simplified case of evolution due only to the $JZ_1 \otimes Z_2$ term. Sandwiching the evolution operator between two rotations $R_x^{(1)}(\pi) = -\mathrm{i}X_1$ of spin 1, we obtain the following effect:

$$\begin{aligned}(-\mathrm{i}X_1)[\exp(-\mathrm{i}Jt\,Z_1 \otimes Z_2)](-\mathrm{i}X_1) &= (-\mathrm{i}X_1)(I_{12}\cos Jt - \mathrm{i}(Z_1 \otimes Z_2)\sin Jt)(-\mathrm{i}X_1) \\ &= I_{12}\cos Jt + \mathrm{i}(Z_1 \otimes Z_2)\sin Jt \\ &= \exp(+\mathrm{i}Jt\,Z_1 \otimes Z_2).\end{aligned} \tag{6.16}$$

Therefore, if the spins have evolved during a time t as $\exp(-\mathrm{i}Jt\,Z_1 \otimes Z_2)$, we obtain the result

$$R_x^{(1)}(\pi)\,[\exp(-\mathrm{i}JtZ_1 \otimes Z_2)]\,R_x^{(1)}(\pi)\,[\exp(-\mathrm{i}JtZ_1 \otimes Z_2)] = I_{12}. \tag{6.17}$$

In other words, the sequence of operations corresponding to free evolution during a time $t \times R_x^{(1)}(\pi) \times$ time evolution during a time $t \times R_x^{(1)}(\pi)$ puts the spins back in their initial configuration! This observation shows how it is possible to cancel

out the evolution of the qubits other than those to which the cNOT gate is applied by means of the operations (6.14) and (6.15). A similar observation reveals how spins which have evolved differently owing to nonuniformities of $\vec{B}_0$ can be refocused.

The molecule (b) of Fig. 6.1 allows us to work with 7 qubits, the minimum number of qubits needed to use the Shor algorithm to factorize 15 into primes. In fact, b can take the values 2, 4, 7, 8, 11, 13, or 14, and the largest period of $b^x \bmod N$ is $r = 4$, for $b = 2$, $b = 7$, $b = 8$ and $b = 13$. To see two periods it is then necessary to take $x = 0, 1, \ldots, 7 = 2^3 - 1$, and of course $f(x) = 0, 1, \ldots, 15 = 2^4 - 1$, that is, a 3-qubit input register and a 4-qubit output register. The factorization of 15 was successfully done in 2001, thanks to the great sophistication of the modern NMR techniques developed for chemical and biological analyses. However, despite this spectacular (?) result, NMR is not the solution of the future, because it first requires the synthesis of a molecule possessing as many distinguishable sites as the needed number of qubits, and the ability to select the frequencies acting on the various qubits. Worst of all, the signal decreases exponentially as the number of qubits grows. In fact, NMR uses not individual quantum objects, but a set of $\gtrsim 10^{18}$ active molecules diluted in a solvent: the signal is a *collective* one. To obtain a "pseudo-pure" state it is necessary to perform preliminary initialization operations too complex to be described here, and the same for measuring the final states. It is these operations which cause the signal to fall off as the number of qubits is increased.

6.2 Trapped ions

Trapped ions represent a more promising technique than NMR. The two states of a qubit are carried by the ground state ($|g\rangle \equiv |0\rangle$) of an ion and by an excited state of very long ($\sim$1 s) lifetime $|e\rangle \equiv |1\rangle$, which is either a hyperfine state of the electronic ground state, or a metastable electronic state. These states will be called *internal states* of the ions. The individual qubits are manipulated by laser pulses, as explained in Section 3.3. The construction of entangled states and two-qubit logic gates involves as an intermediary the translational motion, called the *external degrees of freedom* of the ions. A coupling between the internal and external degrees of freedom is therefore used. Since the ions are trapped in a harmonic potential, we shall speak of vibrational motion of the ions rather than translational motion.

The traps which are used, named Paul traps after their inventor, are constructed by combining the actions of constant and alternating electric fields. The net result

is that the ions are located in a harmonic potential

$$V(x, y, z) = \frac{1}{2} M \left(\omega_x^2 x^2 + \omega_y^2 y^2 + \omega_z^2 z^2\right),$$

where M is the ion mass and $\vec{r} = (x, y, z)$ is the position of the ion in the trap. In practice, the trap frequencies, typically a few megahertz, satisfy the equation

$$\omega_x^2 \sim \omega_y^2 \gg \omega_z^2,$$

so that in a first approximation the ion moves along the axis Oz in a potential

$$V(z) = \frac{1}{2} M\omega_z^2 z^2. \tag{6.18}$$

To start with an elementary discussion, it is useful first to study the case of a single trapped ion. In quantum physics, the z coordinate and the z component of the momentum, p_z, are Hermitian operators (physical properties) satisfying the commutation relation

$$[z, p_z] = \mathrm{i}\hbar I. \tag{6.19}$$

The Hamiltonian $\hat{H}$ with the potential energy term (6.18) also contains a kinetic energy term $p_z^2/2M$:

$$\hat{H} = \frac{p_z^2}{2M} + \frac{1}{2} M\omega_z^2 z^2. \tag{6.20}$$

There exists a standard method for finding the eigenvalues (energy levels) and eigenvectors (stationary states) of $\hat{H}$. One introduces the (dimensionless) operator a and its Hermitian conjugate $a^\dagger$:

$$a = \sqrt{\frac{M\omega_z}{2\hbar}} \left(z + \frac{\mathrm{i}p_z}{M\omega_z}\right), \qquad a^\dagger = \sqrt{\frac{M\omega_z}{2\hbar}} \left(z - \frac{\mathrm{i}p_z}{M\omega_z}\right). \tag{6.21}$$

Using (6.19), it can immediately be checked (Exercise 6.5.2) that a and $a^\dagger$ satisfy the commutation relation

$$\left[a, a^\dagger\right] = I, \tag{6.22}$$

and that $\hat{H}$ can be rewritten as

$$\hat{H} = \hbar\omega_z \left(a^\dagger a + \frac{1}{2}\right). \tag{6.23}$$

It is shown in any quantum mechanics text that the eigenvalues of $\hat{H}$ are of the form $\hbar\omega_z(m + 1/2)$, $m = 0, 1, 2, \ldots$, corresponding to the eigenvectors $|m\rangle$:

$$\hat{H}|m\rangle = \hbar\omega_z \left(m + \frac{1}{2}\right)|m\rangle. \tag{6.24}$$

In general, the operator a (the annihilation operator) takes m to $m-1$, and the operator $a^\dagger$ (the creation operator) takes m to $m+1$:

$$a|m\rangle = \sqrt{m}\,|m-1\rangle, \qquad a^\dagger|m\rangle = \sqrt{m+1}\,|m+1\rangle. \tag{6.25}$$

The integer m therefore labels the vibrational quantum number in the trap. According to (6.25), the ground state $|0\rangle$ is "annihilated" by a: $a|0\rangle = 0$. Its energy E_0 is nonzero: $E_0 = \hbar\omega_z/2$, in contrast to the classical case where the ground state corresponds to an ion at rest in the bottom of the potential well at $z = 0$. The fact that the ground-state energy is nonzero has an interesting physical interpretation in terms of the Heisenberg inequalities (Exercise 2.6.5). Reasoning heuristically, we can replace z and p_z by their dispersions Δz and Δp_z, and use the Heisenberg inequality in the form $\Delta z\,\Delta p_z \sim \hbar/2$ in (6.20) to obtain

$$E \sim \frac{(\Delta p_z)^2}{2M} + \frac{1}{2}M\omega^2(\Delta z)^2 \sim \frac{1}{8M(\Delta z)^2} + \frac{1}{2}M\omega^2(\Delta z)^2.$$

Minimizing with respect to Δz, we find

$$(\Delta z)^2 = \frac{\hbar}{2M\omega_z}, \qquad E_0 = \frac{\hbar}{2}\omega_z, \tag{6.26}$$

in agreement (accidentally – we expected to obtain only the correct order of magnitude) with the exact calculation. This heuristic argument shows that the ground-state energy is obtained by seeking the best compromise between the kinetic energy and the potential energy. They cannot both vanish as in the classical case. The argument also shows that the spread of the ion wave function in the trap, that is, the region where the ion has an appreciable probability of being located, is of order $\Delta z_0 = \sqrt{\hbar/2M\omega_z}$. It is usual to redefine the zero of the vibrational energy such that the ground state has zero energy. Then the energies take the simple form $m\hbar\omega_z$.

There is one final experimental condition to be satisfied. In order to be able to manipulate the ion, it must be in its vibrational ground state $m = 0$. This will not be the case if the ion is at a temperature T such that $k_B T \gtrsim \hbar\omega_z$. In that case, levels with $m \neq 0$ will be thermally excited, and it becomes essential to cool the ions. This is done by Doppler cooling based on the following principle. The ion is sandwiched between two laser beams propagating in opposite directions[6] and tuned to slightly below a resonance frequency. When an ion travels opposite to the direction of one of the laser beams, the transition becomes closer to resonance owing to the Doppler effect, because the ion "sees" more energetic photons, and the absorption of photons from this beam becomes more important than that of photons from the second beam, which the ion "sees" as farther from resonance.

[6] For simplicity, we take the one-dimensional case. Cooling in three dimensions would require six laser beams.

The ion is therefore slowed down no matter what the direction of its velocity is, and it can be shown that the temperature the ion reaches is given by $k_B T \simeq \hbar\Gamma$, where Γ is the linewidth. If the Doppler cooling is insufficient, other more sophisticated mechanisms can be used.

First let us model the ion by a two-level system trapped in the potential (6.18) and located in an oscillating electric field:

$$\vec{E} = E_1 \hat{x} \cos(\omega t - kz - \phi). \tag{6.27}$$

Under these conditions, the total Hamiltonian contains three terms. The first, $\hat{H}_0$, is the Hamiltonian in the absence of the oscillating field ($E_1 = 0$):

$$\hat{H}_0 = -\frac{\hbar}{2}\omega_0 \sigma_z + \hbar\omega_z a^\dagger a. \tag{6.28}$$

The internal states are the two states $|0\rangle$ of energy $-\hbar\omega_0/2$ and $|1\rangle$ of energy $\hbar\omega_0/2$. We shall use the Hamiltonian (6.28) to define a "rotating frame," generalizing what we did in the NMR case.[7] Given an operator A, the operator $\tilde{A}(t)$ will be, by definition,

$$\tilde{A}(t) = e^{i\hat{H}_0 t/\hbar} A\, e^{-i\hat{H}_0 t/\hbar}. \tag{6.29}$$

Following the method of the preceding section,[8] we easily find for the operators a, $a^\dagger$, σ_-, and σ_+ (Exercise 6.5.2):

$$\begin{aligned} \tilde{\sigma}_+(t) &= \sigma_+ e^{-i\omega_0 t}, & \tilde{\sigma}_-(t) &= \sigma_- e^{i\omega_0 t}, \\ \tilde{a}(t) &= a\, e^{-i\omega_z t}, & \tilde{a}^\dagger(t) &= a^\dagger e^{i\omega_z t}. \end{aligned} \tag{6.30}$$

According to (6.27), the interaction with the electric field is written as

$$\hat{H}_{\text{int}} = -\frac{\hbar}{2}\omega_1 \left[\sigma_+ + \sigma_-\right]\left[e^{i(\omega t - \phi)} e^{-ikz} + e^{-i(\omega t - \phi)} e^{ikz}\right],$$

where ω_1 is the Rabi frequency of the problem. In this equation z is the position *operator*. We expand $\exp(\pm ikz)$ in a series keeping only the first two terms:

$$e^{\pm ikz} \simeq 1 \pm ikz,$$

which is valid if $k\Delta z_0 \ll 1$, where $\Delta z_0 = \sqrt{\hbar/2M\omega_z}$ is the spread of the ground-state wave function $m = 0$ in the trap. The condition for the expansion to be valid then is

$$\frac{k\sqrt{\hbar}}{\sqrt{2M\omega_z}} = k\Delta z_0 = \eta \ll 1,$$

[7] The reader familiar with quantum mechanics will recognize (6.29) as the definition of the interaction picture.
[8] However, we choose ω_0 as the rotational frequency of the rotating frame. In fact, it is more convenient to use $\hat{H}_0$ in this problem.

https://doi.org/10.1017/CBO9780511755361.008

where η is called the *Lamb–Dicke* parameter. The term 1 in the expansion of $\exp(\pm \mathrm{i}kz)$ gives a contribution $\hat{H}_1$ to $\hat{H}_{\text{int}}$:

$$\hat{H}_1 = -\frac{\hbar}{2}\omega_1 \left[\sigma_+ + \sigma_-\right]\left[\mathrm{e}^{\mathrm{i}(\omega t-\phi)} + \mathrm{e}^{-\mathrm{i}(\omega t-\phi)}\right].$$

In the rotating frame using the first line of (6.30) we find

$$\hat{H}_1 \to \tilde{H}_1 = -\frac{\hbar}{2}\omega_1 \left[\sigma_+ \mathrm{e}^{-\mathrm{i}\omega_0 t} + \sigma_- \mathrm{e}^{\mathrm{i}\omega_0 t}\right]\left[\mathrm{e}^{\mathrm{i}(\omega t-\phi)} + \mathrm{e}^{-\mathrm{i}(\omega t-\phi)}\right].$$

Finally, we use the *rotating-wave approximation*, where we neglect the terms in $\exp[\pm \mathrm{i}(\omega+\omega_0)t]$ which oscillate rapidly so that they average to zero and give a negligible contribution to the evolution. This leads to the final form:

$$\tilde{H}_1 \simeq -\frac{\hbar}{2}\omega_1 \left[\sigma_+ \mathrm{e}^{\mathrm{i}(\delta t-\phi)} + \sigma_- \mathrm{e}^{-\mathrm{i}(\delta t-\phi)}\right] \tag{6.31}$$

with $\delta = (\omega - \omega_0)$. This is the NMR Hamiltonian (6.4) in the rotating frame, where we have included additional phase factors $\exp(\pm \mathrm{i}\phi)$. It allows us to manipulate the two ion states exactly as in the case of NMR, by tuning the frequency of the oscillating field to $\omega = \omega_0\,(\delta = 0)$ and adjusting the duration of the interaction. The angle defining the rotational axis in the xOy plane can be chosen using the phase ϕ. In fact, at resonance $(\delta = 0)$ the rotation operator is, according to (6.31) with $\theta = -\omega_1 t$,

$$\exp\left(-\mathrm{i}\frac{\theta}{2}\left[\sigma_+ \mathrm{e}^{-\mathrm{i}\phi} + \sigma_- \mathrm{e}^{\mathrm{i}\phi}\right]\right) = \exp\left(-\mathrm{i}\frac{\theta}{2}\left[\sigma_x \cos\phi + \sigma_y \sin\phi\right]\right),$$

which gives a rotation about the axis $\hat{n}$ with the components

$$\hat{n}_x = \cos\phi, \qquad \hat{n}_y = \sin\phi, \qquad \hat{n}_z = 0.$$

In fact, the value of the angle ϕ obviously has no absolute meaning, but in a series of several successive pulses it is the relative phases of the various pulses which are important. In what follows, we can choose an arbitrary value for ϕ. We have kept ϕ explicitly to make the link with Exercise 6.5.3, where it plays an essential role.

The term $\pm \mathrm{i}kz$ in the expansion of the exponential $\exp(\pm \mathrm{i}kz)$ gives a contribution $\hat{H}_2$ to the interaction Hamiltonian. This term takes into account the vibrational motion and couples the internal and external degrees of freedom:

$$\hat{H}_2 = \frac{\mathrm{i}\hbar\eta\omega_1}{2}\left[\sigma_+ + \sigma_-\right]\left[a + a^\dagger\right]\left[\mathrm{e}^{\mathrm{i}(\omega t-\phi)} - \mathrm{e}^{-\mathrm{i}(\omega t-\phi)}\right], \tag{6.32}$$

where we have used (6.21) in the form

$$z = \sqrt{\frac{\hbar}{2M\omega_z}}\left(a + a^\dagger\right).$$

https://doi.org/10.1017/CBO9780511755361.008

In the rotating frame the Hamiltonian $\hat{H}_2$ becomes

$$\begin{aligned}\hat{H}_2 \to \tilde{H}_2 = \frac{\mathrm{i}\eta\hbar\omega_1}{2}\Big[&\sigma_+ a\,\mathrm{e}^{-\mathrm{i}(\omega_0+\omega_z)t} + \sigma_+ a^\dagger\,\mathrm{e}^{-\mathrm{i}(\omega_0-\omega_z)t} \\ &+ \sigma_- a\,\mathrm{e}^{\mathrm{i}(\omega_0-\omega_z)t} + \sigma_- a^\dagger\,\mathrm{e}^{\mathrm{i}(\omega_0+\omega_z)t}\Big] \\ &\times\Big[\mathrm{e}^{\mathrm{i}(\omega t-\phi)} - \mathrm{e}^{-\mathrm{i}(\omega t-\phi)}\Big].\end{aligned}$$

If we choose to tune the laser frequency to $\omega = (\omega + \omega_z)$, the so-called blue side-band frequency, $\tilde{H}_2$ becomes the following in the rotating-wave approximation:

$$\hat{H}_2 \to \tilde{H}_2 = \frac{\mathrm{i}\eta\hbar\omega_1}{2}\Big[\sigma_+ a\,\mathrm{e}^{-\mathrm{i}\phi} - \sigma_- a^\dagger \mathrm{e}^{\mathrm{i}\phi}\Big], \tag{6.33}$$

whereas if we choose $\omega = (\omega_0 - \omega_z)$, the so-called red side-band frequency, we have

$$\hat{H}_2 \to \tilde{H}_2 = \frac{\mathrm{i}\eta\hbar\omega_1}{2}\Big[\sigma_+ a^\dagger \mathrm{e}^{-\mathrm{i}\phi} - \sigma_- a\,\mathrm{e}^{\mathrm{i}\phi}\Big]. \tag{6.34}$$

We use $|n, m\rangle$ to denote the ion state, where $n = 0, 1$ is the internal state and $m = 0, 1$ is the vibrational state of the harmonic oscillator. The Hamiltonian (6.33) induces transitions between the states $|0, 0\rangle$ and $|1, 1\rangle$, because

$$\omega = \omega_0 + \omega_z : \qquad \sigma_+ a|1, 1\rangle = |0, 0\rangle, \qquad \sigma_- a^\dagger|0, 0\rangle = |1, 1\rangle,$$

whereas (6.34) induces transitions between the states $|0, 0\rangle$ and $|1, 1\rangle$, because

$$\omega = \omega_0 - \omega_z : \qquad \sigma_+ a^\dagger|1, 0\rangle = |0, 1\rangle, \qquad \sigma_- a|0, 1\rangle = |1, 0\rangle.$$

This is summarized by the level scheme shown in Fig. 6.3(a).

In order to explain in a simple way how (6.33) and (6.34) can lead to the formation of entangled states, it is convenient to assume the existence of an auxiliary *internal* state $|2\rangle$. It is possible to do without this auxiliary state, but then the discussion is a bit more complicated; see Exercise 6.5.3. We use $|n, m\rangle$ to denote the ion state, $n = 0, 1, 2$ being the internal (spin) state and m the excitation state of the harmonic oscillator. We then obtain the level scheme of Fig. 6.3(b). The four basis states for the quantum calculation are $|0, 0\rangle$, $|0, 1\rangle$, $|1, 0\rangle$ and $|1, 1\rangle$, and we need to construct two-qubit logic gates for these states. A laser is tuned to the frequency $(\omega_{\mathrm{aux}} + \omega_z)$, thus stimulating transitions between the states $|2, 0\rangle$ and $|1, 1\rangle$, corresponding to an effective Hamiltonian

$$\hat{H}_{\mathrm{aux}} = \mathrm{i}\frac{\eta\hbar\omega_1'}{2}\Big[\sigma_+' a\,\mathrm{e}^{\mathrm{i}\phi} - \sigma_-' a^\dagger \mathrm{e}^{-\mathrm{i}\phi}\Big] \tag{6.35}$$

with

$$\sigma_+'|1\rangle = |2\rangle, \qquad \sigma_-'|2\rangle = |1\rangle.$$

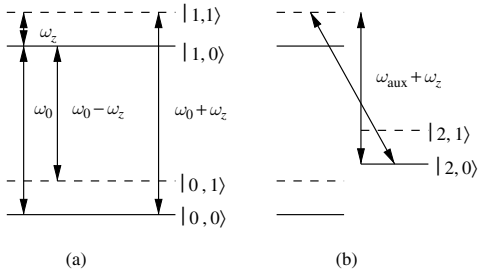

Figure 6.3 (a) Energy levels of the simplified model for the coupling of the internal and external degrees of freedom. The states are labeled $|n, m\rangle$, where $n = 0, 1$ is the state of the qubit (internal) and m is the vibrational quantum number (external). (b) Coupling to an auxiliary level: now n can take the values 0, 1, and 2, with m always denoting the vibrational quantum number. The transition at $\omega_0 - \omega_z$ corresponds to the red side-band, and that at $\omega_0 + \omega_z$ to the blue side-band.

The laser is applied during the time needed to perform a rotation $R_x(2\pi)$, the effect of which is $|1, 1\rangle \to -|1, 1\rangle$ with the other states remaining unchanged. This realizes the cZ logic gate on the states $|n, m\rangle$:

$$\mathrm{cZ} = \begin{pmatrix} 1 & 0 & 0 & 0 \\ 0 & 1 & 0 & 0 \\ 0 & 0 & 1 & 0 \\ 0 & 0 & 0 & -1 \end{pmatrix} = \begin{pmatrix} I & 0 \\ 0 & \sigma_z \end{pmatrix}. \tag{6.36}$$

Let us now turn to the more interesting case of two ions. The arguments can be generalized immediately to any number of ions N, which allows us (in theory!) to imagine a quantum computer with N qubits. As a preliminary result, we need the SWAP gate, obtained by tuning the laser to the red side-band frequency $(\omega - \omega_z)$ and by adjusting the duration of the pulse for a rotation by π. Choosing $\phi = \pi/2$, this gives the exchange $|0, 1\rangle \leftrightarrow |1, 0\rangle$ corresponding to the SWAP logic gate, with an extra minus sign

$$\mathrm{SWAP}' = \begin{pmatrix} 1 & 0 & 0 & 0 \\ 0 & 0 & -1 & 0 \\ 0 & 1 & 0 & 0 \\ 0 & 0 & 0 & 1 \end{pmatrix}. \tag{6.37}$$

The vibrational ground state corresponds to motion of the ensemble of both ions, that is, to vibration of the center of mass inside the trap. Therefore, everything is the same as for a single ion. The combination of cZ, SWAP, and Hadamard gates gives a cNOT gate. Let us explain how. We choose ion 1 as the control ion and ion 2 as the target ion. It should be borne in mind that the qubits are carried

by the two internal states of these ions. We start from a state which is the tensor product of the most general two-qubit state

$$a|00\rangle + b|01\rangle + c|10\rangle + d|11\rangle$$

and of the state corresponding to the $m = 0$ vibrational mode of the center of mass:

$$\begin{aligned}
\text{initial} &: (a|00\rangle + b|01\rangle + c|10\rangle + d|11\rangle) \otimes |0\rangle \\
&= a|00, 0\rangle + b|01, 0\rangle + c|10, 0\rangle + d|11, 0\rangle \\
\text{SWAP}'_2 &: a|00, 0\rangle + b|00, 1\rangle + c|10, 0\rangle + d|10, 1\rangle \\
\text{cZ}_1 &: a|00, 0\rangle + b|00, 1\rangle + c|10, 0\rangle - d|10, 1\rangle \\
\text{SWAP}'_2 &: a|00, 0\rangle - b|01, 0\rangle + c|10, 0\rangle + d|11, 0\rangle \\
&= (a|00\rangle - b|01\rangle + c|10\rangle + d|11\rangle) \otimes |0\rangle.
\end{aligned}$$

If we redefine the phase of the state $|1\rangle_2$ of the second ion, $|1\rangle_2 \to -|1\rangle_2$, the net result is the application of a cZ gate to the two qubits: the vibrational motion has only served as an intermediary. It is easy to go from a cZ gate to a cNOT gate, as we have seen in (6.15). This gate has been realized experimentally using as qubits the ground state $S_{1/2}$ ($|g\rangle \equiv |0\rangle$) and the metastable state $D_{5/2}$ ($|e\rangle \equiv |1\rangle$, of lifetime of the order of a second) of the $^{40}Ca^+$ ion; the transition between the two levels is an electric quadrupole transition corresponding to a wavelength of 729 nm. An N-qubit computer is shown schematically in Fig. 6.4.

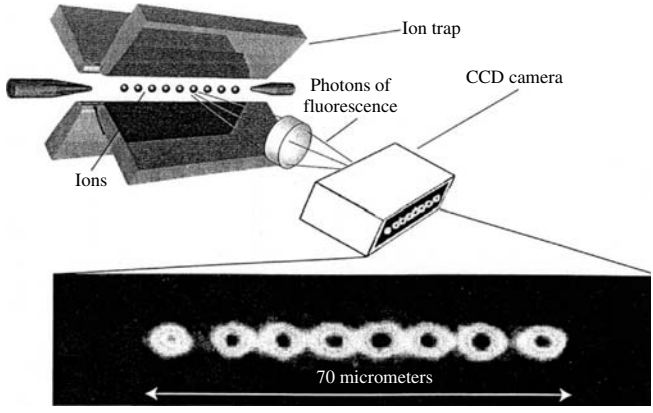

Figure 6.4 Schematic depiction of the principle of a quantum computer using N trapped ions. From Aspect and Grangier (2004).

The potential energy V of the ensemble of N ions in the trap is

$$V = \frac{1}{2} M \sum_{n=1}^{N} \omega_z^2 z_n^2 + \frac{q^2}{4\pi\varepsilon_0} \sum_{m \neq n} \frac{1}{|z_n - z_m|}, \tag{6.38}$$

assuming that the ion chain is linear: the trap potential must be sufficiently confining in the directions Ox and Oy in order to avoid zig-zag configurations. The minimum distance between the ions at equilibrium, which is the distance between the two central ions, is approximately

$$\Delta z \simeq 2lN^{-0.057},$$

where l is the characteristic length of the problem:

$$l = \left(\frac{q^2}{4\pi\varepsilon_0 M \omega_z^2} \right)^{1/3}. \tag{6.39}$$

For the trap of the Innsbruck group the numerical value is $l \simeq 2.8\,\mu\text{m}$, the central ions being separated by about $5\,\mu\text{m}$. The lowest vibrational mode of frequency ω_z corresponds to motion of the ensemble of ions, and the first excited mode, or the breathing mode of frequency $\sqrt{3}\omega_z$, corresponds to the ions oscillating with amplitude proportional to their algebraic distance from the center of the trap (Exercise 6.5.4). One of the delicate problems is how to address an individual ion by a laser beam – it is necessary to aim very accurately!

A resonance fluorescence technique is used to put the ions in the desired state and to measure their final state $|g\rangle := |0\rangle$ or $|e\rangle := |1\rangle$. The ions are illuminated by a laser beam tuned to an electric dipole transition between the level $|g\rangle$ and an excited level $|r\rangle$, $|g\rangle \leftrightarrow |r\rangle$. If the ion is in the state $|g\rangle$, it will scatter a large number of photons, while if it is in the state $|e\rangle$ it will not. The quantum jumps made by the ions in this method are quite spectacular, because the observation is made for an *individual* quantum system. One main difficulty of trapped ions is that ions are charged particles, and as such are sensitive to stray electric fields. If these fields are time dependent, they will heat the ions. Typical heating times are of the order of 1 ms, but this time could be much shorter as the number of ions increases.

6.3 Superconducting qubits

In the two preceding examples the qubits were carried by individual quantum objects, nuclear spins in the NMR case and ions in the case of trapped ions (although in the NMR case the signal was built up by $\sim 10^{18}$ nuclear spins). We now turn to a system where the qubits are carried by a macroscopic degree of freedom, the current in a superconducting circuit containing one or several

https://doi.org/10.1017/CBO9780511755361.008

Josephson junctions. As we shall see, low temperatures of the order of tens of millikelvins are required for these circuits to exhibit quantum behavior. These circuits are small by everyday standards (a few micrometers), but very large compared to atomic sizes. Still more remarkable is the fact that the parameters of these quantum systems are fixed by fabrication, and not by Nature as is the case for individual quantum systems like electrons or ions. They are engineered quantities which can be modified by changing the dimensions of the circuits, and in this sense they are unambiguously macroscopic quantities. It has been known for almost a century that at low temperatures the electrical resistance of most metals and alloys drops abruptly to zero below a transition temperature T_C of order 1 K, and the metal becomes a superconductor. Superconductors also exhibit a remarkable feature called the Meissner effect: magnetic fields are expelled from the bulk of a superconductor; they cannot penetrate deeper than a distance known as the London penetration length,[9] which is of order 0.1 μm.

In order first to examine a simple example, which, however, will turn out not to be suitable for qubits, consider the LC circuit of Fig. 6.5 at very low temperatures, so that all metallic elements are superconducting. The classical Hamiltonian of the oscillator is the sum of the magnetic energy stored in the inductor and the electrical energy stored in the capacitor:

$$H = \frac{1}{2L}\varphi^2 + \frac{1}{2C}q^2, \tag{6.40}$$

where L and C are the inductance and the capacitance, φ is the flux across the inductor, and q is the charge on the capacitor. The resonance frequency of the circuit is $\omega_0 = \sqrt{LC}$. The circuit of Fig. 6.5 can be fabricated with lateral

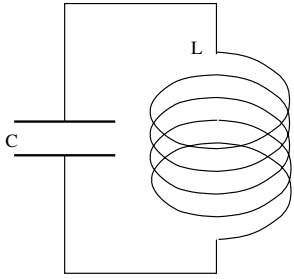

Figure 6.5 A superconducting LC circuit.

[9] We limit ourselves to the so-called type I superconductors, or to type II superconductors in external magnetic fields smaller than the critical field H_{C_1}. We also exclude from our discussion high-T_C superconductors, where the transition temperature can reach ∼100 K. In contrast to low-temperature superconductors, which are very well described by the Bardeen–Cooper–Schrieffer (BCS) theory, high-T_C superconductors are still poorly understood.

dimensions $\simeq 10\,\mu\text{m}$, with values of L and C approximately 0.1 nH and 1 pF, respectively, corresponding to a resonance frequency $\omega_0/2\pi \simeq 16\,\text{GHz}$. When aluminum with $T_C = 1.1\,\text{K}$ is used to fabricate the circuit one can safely neglect dissipation due to unpaired electrons (quasi-particles) below [10] 20 mK.

The magnetic flux φ and the charge q in (6.40) may be considered as conjugate variables in the sense of analytical mechanics: the Hamiltonian (6.40) has the same form as (6.20) if we make the substitutions $p_z \to \varphi$, $M \to L$, $z \to q$, and $M\omega_z^2 \to 1/C$. The correspondence principle tells us how to quantize the circuit. As in the case of the variables z and p_z, the classical variables (numbers) q and φ become operators Q and Φ which obey the canonical commutation relation $[Q, \Phi] = \mathrm{i}\hbar I$. However, we know that under ordinary conditions quantum effects are (fortunately) quite negligible in electrical circuits. So when do quantum effects begin to play a role? As in the case of trapped ions, the thermal energy $k_B T$ must be much smaller than the energy difference between the ground and first excited states. According to the results described in the preceding section on the quantum harmonic oscillator, here this energy difference is $\hbar\omega_0$, and quantum effects are relevant for the circuit of Fig. 6.5 when

$$k_B T \ll \hbar\omega_0. \tag{6.41}$$

Unfortunately, this simple circuit is not suitable as a support for qubits. The reason is that the energy difference between the first and second excited states is also $\hbar\omega_0$, so that any attempt to produce Rabi oscillations between the ground and first excited levels will unavoidably induce transitions to the second excited and higher levels, so that there is no possibility of a two-level system. The equal spacing $\hbar\omega_0$ between the harmonic oscillator quantum levels can be traced back to the linearity of the oscillator. We thus need to introduce strong nonlinear effects, and the only known device which is able to create strong nonlinearities without dissipation is the Josephson junction.

In a superconductor the electrons are weakly bound in pairs, called Cooper pairs, of zero spin and zero momentum at equilibrium. At zero temperature all these pairs "condense," that is, they all fall into the same state, the ground state, so that all pairs have the same wave function. [11] The energy needed to break one of the pairs is called the gap energy Δ, and it is the energy difference between the ground and first excited states. In contrast to a single-electron wave function, which is a probability amplitude whose modulus squared gives the *probability*

[10] As explained below, the characteristic energy is the gap energy Δ, and dissipation due to unpaired electrons is negligible if $k_B T \ll \Delta$, because the residual resistance decreases as $\sim \exp(-\Delta/k_B T)$. The value of the gap for aluminum is $\Delta \simeq 200\,\mu\text{eV}$, and the number of quasi-particles in a typical circuit at 20 mK is less than 10^{-10}.

[11] This phenomenon is known as the Bose–Einstein condensation of bosons. Electrons are fermions, not bosons, but Cooper *pairs* do behave as bosons.

density of finding the electron at some point in space, the wave function of the condensed state, as it involves a macroscopic number of pairs, may be interpreted in terms of a Cooper pair density $\rho(\vec{r})$. More precisely, this macroscopic wave function is a complex function which can be written as

$$\psi(\vec{r}) = \sqrt{\rho(\vec{r})}\, \mathrm{e}^{\mathrm{i}\theta(\vec{r})}, \tag{6.42}$$

so that $|\psi(\vec{r})|^2 = \rho(\vec{r})$ is the Cooper pair density at the point $\vec{r}$ and $\theta(\vec{r})$ is the phase. In a uniform situation ρ and θ are independent of $\vec{r}$. The Meissner effect is explained by starting from the standard form of the electromagnetic current in quantum mechanics for a particle of charge q and mass m under the influence of a magnetic field $\vec{B}$ derived from a vector potential $\vec{A}(\vec{r})$ ($\vec{B} = \vec{\nabla} \times \vec{A}$):

$$\begin{aligned} \vec{J}_{\mathrm{em}} &= \frac{q}{2m}\left[\psi^*(\vec{r})\left(-\mathrm{i}\hbar\vec{\nabla} - q\vec{A}(\vec{r})\right)\psi + \psi(\vec{r})\left(\mathrm{i}\hbar\vec{\nabla} - q\vec{A}(\vec{r})\right)\psi^*\right] \\ &= \frac{\hbar q}{m}\left(\vec{\nabla}\theta(\vec{r}) - \frac{q}{\hbar}\vec{A}(\vec{r})\right)\rho(\vec{r}). \end{aligned} \tag{6.43}$$

This expression can be used to show that the magnetic field cannot penetrate the bulk of the superconductor, but must decrease exponentially from its surface (Exercise 6.5.5). Another crucial consequence of (6.43) is that the magnetic flux φ through a superconductor ring is quantized due to the fact that currents must flow at the surface of the superconductor (Exercise 6.5.5). Indeed, considering a contour drawn inside the ring along which the current density vanishes, from $\vec{J}_{\mathrm{em}} = 0$ and from the fact that the wave function is single valued we find

$$\oint \vec{\nabla}\theta \cdot \mathrm{d}l = \frac{q_{\mathrm{C}}}{\hbar}\oint \vec{A}\cdot\mathrm{d}\vec{l} = \frac{q_{\mathrm{C}}}{\hbar}\int\int \vec{B}\cdot\mathrm{d}\vec{\mathcal{S}} = 2\pi n, \qquad n \in \mathbb{Z},$$

so that

$$\int\int \vec{B}\cdot\mathrm{d}\vec{\mathcal{S}} = \frac{\hbar}{q_{\mathrm{C}}}\,2\pi n = n\varphi_0 \tag{6.44}$$

where q_{C} is the charge of the Cooper pair, $q_{\mathrm{C}} = 2q_{\mathrm{e}}$, q_{e} being the electron charge. The elementary *flux quantum* $\varphi_0 = 2\pi\hbar/q_{\mathrm{C}}$, $|\varphi_0| \simeq 2 \times 10^{-15}$ Wb, plays an important role in what follows.

A Josephson junction (Fig. 6.6) is made of two superconductors which are separated by a layer of insulating material. If the layer is thick the electrons cannot cross it, but if it is thin enough they can get across owing to a quantum process known as tunneling. If ψ_1 (ψ_2) is the macroscopic wave function (6.42) on the right (left) side of the junction, to which a bias voltage V is applied, we

https://doi.org/10.1017/CBO9780511755361.008

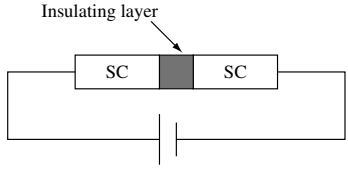

Figure 6.6 Schematic depiction of a Josephson junction: a thin insulating layer is sandwiched between two superconducting (SC) wires.

can describe the junction as a two-level system, and by analogy with (3.30) we can write down a system of coupled differential equations for ψ_1 and ψ_2:

$$\begin{aligned} \mathrm{i}\hbar\frac{\mathrm{d}\psi_1}{\mathrm{d}t} &= \frac{1}{2}\,q_{\mathrm{C}}V\psi_1 + K\psi_2, \\ \mathrm{i}\hbar\frac{\mathrm{d}\psi_2}{\mathrm{d}t} &= -\frac{1}{2}\,q_{\mathrm{C}}V\psi_2 + K\psi_1. \end{aligned} \tag{6.45}$$

The coupling between the two wave functions is due to tunneling and is characterized by an amplitude K which may be chosen to be real. The factors $\pm q_{\mathrm{C}}V/2$ can be understood as follows. In the absence of coupling ($K = 0$) the functions ψ_1 and ψ_2 are energy eigenstates whose time evolution is $\exp(\pm \mathrm{i}q_{\mathrm{C}}Vt/2\hbar)$ since the energy of a Cooper pair is $\pm q_{\mathrm{C}}V/2$. Writing ψ_1 and ψ_2 in the form (6.42)

$$\psi_1 = \sqrt{\rho_1}\,\mathrm{e}^{\mathrm{i}\theta_1}, \qquad \psi_2 = \sqrt{\rho_2}\,\mathrm{e}^{\mathrm{i}\theta_2}, \tag{6.46}$$

we obtain a system of coupled equations for the quantities ρ_1, ρ_2, θ_1, and θ_2. After some simple algebra (see Exercise 6.5.6), we find that the Josephson current I_{J} across the junction is

$$I_{\mathrm{J}} = \frac{2K}{\hbar}\sqrt{\rho_1\rho_2}\,\sin\theta = I_0\sin\theta, \tag{6.47}$$

where $\theta = \theta_2 - \theta_1$ is the phase difference across the junction. I_0 is called the critical current, and it is a parameter characteristic of the junction. The phase difference is governed by the equation (Exercise 6.5.6)

$$V = \frac{\hbar}{q_{\mathrm{C}}}\frac{\mathrm{d}\theta}{\mathrm{d}t} = \frac{\varphi_0}{2\pi}\frac{\mathrm{d}\theta}{\mathrm{d}t}. \tag{6.48}$$

Note that in a stationary regime the potential difference across the junction vanishes as long as there is no dissipation in the junction. Equations (6.47) and (6.48) are the fundamental equations of the Josephson effect. These two equations can be combined to obtain

$$\frac{\mathrm{d}I_{\mathrm{J}}}{\mathrm{d}t} = \frac{2\pi}{\varphi_0}\,VI_0\cos\theta. \tag{6.49}$$

This expression can be interpreted as that of an inductor, $\mathcal{E} = L\mathrm{d}I/\mathrm{d}t$, where $\mathcal{E}$ is the emf and L is the inductance, with the effective inductance of the junction given by

$$L_{\mathrm{J}} = \frac{\varphi_0}{2\pi I_0 V \cos\theta}. \tag{6.50}$$

The $1/\cos\theta$ behavior makes it clear that this inductance is highly nonlinear, a property we were looking for. The energy U_{J} stored in the inductor is

$$U_{\mathrm{J}} = \int_{-\infty}^{t} I_{\mathrm{J}}(t')V_{\mathrm{J}}(t')\,\mathrm{d}t' = \frac{I_0\varphi_0}{2\pi}\int_0^{\theta} \sin\theta'\,\mathrm{d}\theta' = -\frac{I_0\varphi_0}{2\pi}\cos\theta = E_{\mathrm{J}}\cos\theta. \tag{6.51}$$

Before discussing the construction of circuits for superconducting qubits, let us describe a simple closed circuit (a ring) built with one Josephson junction, an inductor L, and a capacitor C (Fig. 6.7). The total magnetic flux through the circuit is φ, composed of an external flux φ_{ex} and the flux $(\varphi - \varphi_{\mathrm{ex}})$ due to the inductance. From a slight modification of (6.44) (see Exercise 6.5.5) we deduce that

$$\theta = 2\pi\frac{\varphi}{\varphi_0} + 2n\pi, \qquad n \in \mathbb{Z}, \tag{6.52}$$

so that $\cos\theta$ in (6.51) can be replaced by $\cos(2\pi\varphi/\varphi_0)$. Then the total energy of the circuit, or the Hamiltonian, is

$$H = \frac{1}{2C}q^2 + \frac{1}{2L}(\varphi - \varphi_{\mathrm{ex}})^2 - \frac{I_0\varphi_0}{2\pi}\cos\left(\frac{2\pi\varphi}{\varphi_0}\right) - I_{\mathrm{ex}}\varphi, \tag{6.53}$$

where we have added a possible contribution from an external current I_{ex} arriving at the ring.

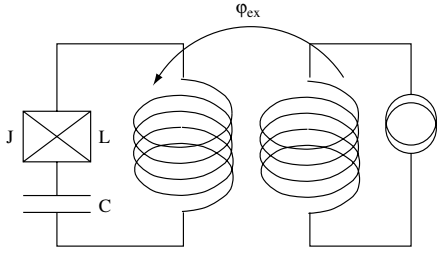

Figure 6.7 A superconducting circuit for flux qubits. J represents the Josephson junction.

As in the case of the LC circuit of Fig. 6.5, we can quantize the Hamiltonian H in (6.53) by using two conjugate operators Q and Φ obeying the commutation relation $[Q, \Phi] = \mathrm{i}\hbar I$. We then write the quantum Hamiltonian $\hat{H}$ as

$$\hat{H} = \frac{1}{2C} Q^2 + \frac{1}{2L} (\Phi - \varphi_{\mathrm{ex}})^2 - \frac{I_0 \varphi_0}{2\pi} \cos\left(\frac{2\pi\Phi}{\varphi_0}\right) - I_{\mathrm{ex}}\Phi. \tag{6.54}$$

A possible realization of the canonical commutation relations is $\Phi \to \varphi$, $Q \to \mathrm{i}\hbar\partial/\partial\varphi$, where the operators Q and Φ act in the Hilbert space of square integrable functions of φ. In this realization of the commutation relations Φ is represented by multiplication by φ, while Q is represented by the differential operator $\mathrm{i}\hbar\partial/\partial\varphi$. Indeed, it can immediately be checked that $[Q, \Phi]$ acting on a function $f(\varphi)$ gives back $\mathrm{i}\hbar f(\varphi)$:

$$[Q, \Phi] f(\varphi) = \mathrm{i}\hbar \frac{\partial(\varphi f)}{\partial\varphi} - \mathrm{i}\hbar\varphi \frac{\partial f}{\partial\varphi} = \mathrm{i}\hbar f(\varphi).$$

The circuit of Fig. 6.7 has been used to explore the boundary between the classical and quantum worlds, as it allows the study of quantum superpositions of macroscopic distinguishable states (see Leggett (2002)). The macroscopic distinct states correspond to currents of order $1\,\mu$A flowing in opposite directions in the ring.

Three different types of circuit with Josephson junctions have been proposed to serve as a support for qubits. At present it is quite impossible to tell which of these circuits (if any!) will turn out to be the most suitable one. We shall limit our discussion to the "flux qubits," leaving the "charge qubits" to Exercise 6.5.7 and the "phase qubits" to the references. The circuit for flux qubits is that of Fig. 6.7, where an external coil is used to generate an external flux φ_{ex}. The quantum Hamiltonian acting on functions $f(\varphi)$ is then

$$\begin{aligned} \hat{H} &= \frac{1}{2C}\left(-\hbar^2 \frac{\partial^2}{\partial\varphi^2}\right) + \frac{1}{2L}(\varphi - \varphi_{\mathrm{ex}})^2 + E_{\mathrm{J}} \cos\left(\frac{2\pi\varphi}{\varphi_0}\right) \\ &= \frac{1}{2C}\left(-\hbar^2 \frac{\partial^2}{\partial\varphi^2}\right) + U(\varphi), \end{aligned} \tag{6.55}$$

with $E_{\mathrm{J}} = -I_0\varphi_0/(2\pi)$ (see (6.51)). The flux φ can take continuous values between $-\infty$ and $+\infty$. The Hamiltonian (6.55) contains three adjustable energy scales: E_{J}, $q_{\mathrm{c}}^2/2C$, and ${\varphi^2}_0/2L$. The flux qubits correspond to the case $E_{\mathrm{J}} \gg q_{\mathrm{C}}^2/2C$, where the phase is well defined and the number of Cooper pairs fluctuates strongly, while the opposite situation holds for the charge qubits. For $\varphi_{\mathrm{ex}} = \varphi_0/2$ it is clear that the potential $U(\varphi)$ in (6.55) is symmetric in the variable $(\varphi - \varphi_0/2)$, and for a suitable choice of the parameters it exhibits a double-well structure (Fig. 6.8). Owing to the symmetry the ground states of the two wells are degenerate. They correspond physically to a macroscopic ($\sim 1\,\mu$A) current flowing around the loop in the clockwise direction (the state $|0\rangle$) and in the counter-clockwise direction (the state $|1\rangle$). These states $|0\rangle$ and $|1\rangle$ will be chosen as the two basis states

https://doi.org/10.1017/CBO9780511755361.008

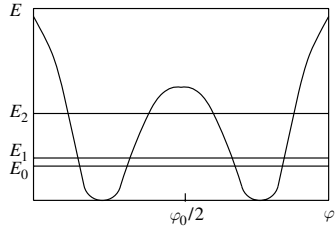

Figure 6.8 The potential $U(\varphi)$ in the symmetric case $\varphi_{\rm ex} = \varphi_0/2$, together with its three lowest levels.

for a qubit. The symmetric double-well potential $U(\varphi)$ in (6.55) is sketched in Fig. 6.8 together with its first three energy levels for $\varphi_{\rm ex} = \varphi_0/2$. The two wells are separated by a barrier, and in classical physics a system with low enough energy would be trapped in one of the two wells. This is not the case in quantum physics, where the system can tunnel from one well to the other. Let c_0 and c_1 be the probability amplitudes for finding the system in the state $|0\rangle$ or $|1\rangle$. In the absence of tunneling, the Schrödinger equation would be simply

$$\mathrm{i}\hbar\dot{c}_0 = E_0 c_0, \qquad \mathrm{i}\hbar\dot{c}_1 = E_0 c_1,$$

where the dynamics of the two states are decoupled and they both have energy E_0. In the presence of tunneling, the two amplitudes will be coupled as

$$\begin{aligned} \mathrm{i}\hbar\frac{\mathrm{d}c_0}{\mathrm{d}t} &= E_0 c_0 - A c_1, \\ \mathrm{i}\hbar\frac{\mathrm{d}c_1}{\mathrm{d}t} &= E_0 c_1 - A c_0, \end{aligned} \tag{6.56}$$

where $A > 0$ is the tunneling amplitude. The two possible values of the energy are $E_0 \mp A$, respectively corresponding to the states $|\pm\rangle$:

$$|\pm\rangle = \frac{1}{\sqrt{2}}(|0\rangle \pm |1\rangle). \tag{6.57}$$

When we move from $\varphi_{\rm ex} = \varphi_0/2$ to other values of $\varphi_{\rm ex}$ the symmetry of $U(\varphi)$ about the point $\varphi = \varphi_0/2$ is lost, and one of the wells becomes deeper than the other. The splitting $2E_{\rm ex}$ between the bottom of the two wells varies linearly with the applied flux

$$E_{\rm ex} = \zeta \frac{\varphi_0^2}{2L}\left(\frac{\varphi_{\rm ex}}{\varphi_0} - \frac{1}{2}\right), \tag{6.58}$$

where ζ is a number which must be computed numerically. In the $|\pm\rangle$ basis, the qubit Hamiltonian may be written in the form

$$\hat{H}_{\rm qubit} = -A\sigma_z + E_{\rm ex}\sigma_x,$$

the eigenvalues of the energies being

$$E_{\pm} = \pm\sqrt{A^2 + E_{\rm ex}^2}.$$

For $E_{\rm ex} = 0$ ($\varphi_{\rm ex} = \varphi_0/2$), $E_{\pm} = \pm A$, while for $|E_{\rm ex}| \gg A$, one has $E_{\pm} \simeq \pm|E_{\rm ex}|$. The level scheme is drawn in Fig. 6.9, where the familiar level repulsion is observed. Instead of crossing at $\varphi_{\rm ex} = \varphi_0/2$, the two levels "avoid" each other (Exercise 6.5.7). The final result for the qubit Hamiltonian can be written in the form

$$\hat{H}_{\rm qubit} = -A(\sigma_z + X\sigma_x),$$
$$X = -\frac{E_{\rm ex}}{A} = -\frac{\zeta}{A}\frac{\varphi_0^2}{2L}\left(\frac{\varphi_{\rm ex}}{\varphi_0} - \frac{1}{2}\right). \tag{6.59}$$

In practice, a circuit with three Josephson junctions instead of one is used in the case of Fig. 6.7. This allows the behavior of the circuit to be fine tuned more easily. It has been possible to demonstrate Rabi oscillations on the flux qubit as well as Ramsey fringes and spin echo, and to perform spectroscopic measurements on two coupled qubits. The readout of the qubits in the case of superconducting qubits is a delicate problem, because the readout device is a source of decoherence. In the flux qubit case, the readout is performed by means of a SQUID which encircles the circuit. A SQUID, which is also constructed from Josephson junctions, is a very sensitive magnetometer, and measurement of the direction of the magnetic field, which is linked to the sense of rotation of the current, allows the qubit state to be deduced. In recent experiments it has been possible to obtain decoherence times $\sim 1\,\mu$s, whereas a gate operation takes a few nanoseconds. Recent experiments have also shown that it is possible to

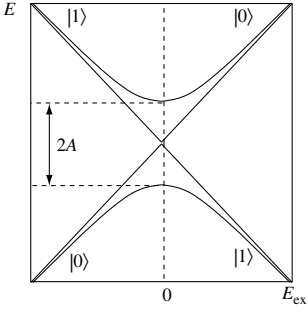

Figure 6.9 The level scheme of the qubit Hamiltonian (6.59). The level repulsion is clearly seen: instead of crossing at $E_{\rm ex} = 0$, the two levels are separated by $2A$. For $|E_{\rm ex}| \gg A$, the eigenstates of $\hat{H}_{\rm qubit}$ are approximately $|0\rangle$ and $|1\rangle$.

couple two superconducting qubits by using a mutual inductance (or capacitance) coupling the two circuits.

6.4 Quantum dots

The amazing progress in the fabrication of small artificial structures in semiconductors has led to an abundance of proposals for solid-state implementations of quantum computers. However, so far none of these proposals has been able to exhibit the concrete realization of a pair of qubits with controlled entanglement together with efficient readout of the final state.

Here we shall consider only one of the most promising schemes, which is based on *quantum dots*. A quantum dot is a structure built in a semiconductor which is able to confine electrons in three dimensions in such a way that discrete energy levels are obtained, much as for an atom; in fact, quantum dots can be regarded as artificial atoms whose characteristics can be controlled by hand. Furthermore, the number of charge carriers in the conduction band of the dot can be very precisely controlled. Quantum dots form spontaneously when semiconductor material is deposited on a substrate with a different lattice spacing. Such a combination is called a heterostructure. The quantum dots have a bowl-like shape, with a typical diameter of 100 nm and a height of 30 nm. The confining potential for charge carriers is approximately a two-dimensional harmonic potential in the horizontal plane.

Two main schemes have been proposed for qubits. The first one is based on excitons, an exciton being an electron–hole pair which is created by light absorption. The exciton energy is $E_{\mathrm{ex}} = E_{\mathrm{g}} - E_{\mathrm{b}}$, where E_{g} is the band gap and E_{b} is the binding energy of the electron–hole pair. The idea is to use two coupled quantum dots to entangle qubits. The electron and the hole can be in one (the state $|0\rangle$) or the other (the state $|1\rangle$) of the quantum dots. Then $|00\rangle$ corresponds to an electron–hole pair in dot 1, $|11\rangle$ to the pair in dot 2, and $|01\rangle$ and $|10\rangle$ to the electron in dot 1 and the hole in dot 2 and vice versa. If the distance between the two dots is of order 5 nm, electrons and holes can tunnel from one dot to the other. As in the case of superconducting qubits, the eigenstates are therefore the symmetric and antisymmetric linear combinations of the states $|0\rangle$ and $|1\rangle$. The readout of the excitonic states is relatively straightforward, at least in principle. The electron–hole pair recombines after a time $\sim$1 ns, and the wavelength of the emitted photon is directly linked to the state occupied by the particles before they recombined.

The second idea is to use electron spin to encode qubits. The first advantage of this scheme is that the Hilbert space for spin is two-dimensional and there is no contamination from other levels. The second one is that decoherence times

can be as long as a few microseconds, because the spins are weakly coupled to their environment. The third one is that spins can in principle be transported along conducting wires within the quantum network. Compared to nuclear spins, electron spins have much stronger couplings to magnetic fields, because the ratio of the proton mass to the electron mass is $\sim 10^3$, and the gyromagnetic ratio (Box 3.1) is inversely proportional to the mass. This feature allows gate operations which are much faster than for NMR. The readout of the final state is probably the most difficult challenge for spin qubits. One possibility might be to convert spin degrees of freedom into charge degrees of freedom, followed by electrical detection. Important progress in readout has been recently achieved by Hanson *et al.* (2005).

The Hamiltonian of a set of electron spins localized in a coupled array of quantum dots can be written as

$$\hat{H} = \sum_{\langle i,j \rangle} J_{ij}(t) \vec{\sigma}_i \cdot \vec{\sigma}_j + \frac{1}{2} \mu_{\mathrm{B}} \sum_i g_i(t) \vec{B}_i(t) \cdot \vec{\sigma}_i, \tag{6.60}$$

where $\vec{\sigma}_i$ is the Pauli spin matrix associated with the ith electron and $\mu_{\mathrm{B}} = q_{\mathrm{e}}\hbar/(2m_{\mathrm{e}})$ is the Bohr magneton. J_{ij} describes the coupling between spins, which may be assumed to be zero unless the spins are nearest neighbors on the array; $\sum_{\langle ij \rangle}$ denotes a sum over nearest neighbors. The second term in (6.60) is the coupling to the external magnetic field $\vec{B}_i(t)$. As in the NMR case, J_{ij} can be used to build two-qubit gates, while $\vec{B}_i(t)$ is used for single-qubit gates. However, in contrast to the NMR case, the exchange interaction $J_{ij}(t)$ is switched on and off adiabatically. Writing $J_{ij}(t) = J_{ij}[v(t)]$, the necessary condition is $|\dot{v}/v| \ll \delta\varepsilon/\hbar$, where $\delta\varepsilon$ denotes the level separation. In order to implement one-qubit gates, it is necessary to address the right qubit. This can be done by varying the magnetic field $B_i(t)$ or the Landé factor $g_i(t)$ in order to make the resonance frequency dependent on the qubit position. From (6.60) we find the two-qubit Hamiltonian in the form

$$\hat{H} = J(t) \vec{\sigma}_1 \cdot \vec{\sigma}_2. \tag{6.61}$$

As shown in Exercise 4.6.4, the operator $\vec{\sigma}_1 \cdot \vec{\sigma}_2$ (up to an additive constant) exchanges the two qubits:

$$\vec{\sigma}_1 \cdot \vec{\sigma}_2 |00\rangle = |00\rangle, \quad \vec{\sigma}_1 \cdot \vec{\sigma}_2 |01\rangle = |10\rangle, \quad \vec{\sigma}_1 \cdot \vec{\sigma}_2 |10\rangle = |01\rangle, \quad \vec{\sigma}_1 \cdot \vec{\sigma}_2 |11\rangle = |11\rangle.$$

This is the SWAP operation already encountered in (6.37). After a π pulse such that

$$\int_0^{\tau_s} \mathrm{d}t J(t) = J_0 \tau_s = \pi \bmod 2\pi \tag{6.62}$$

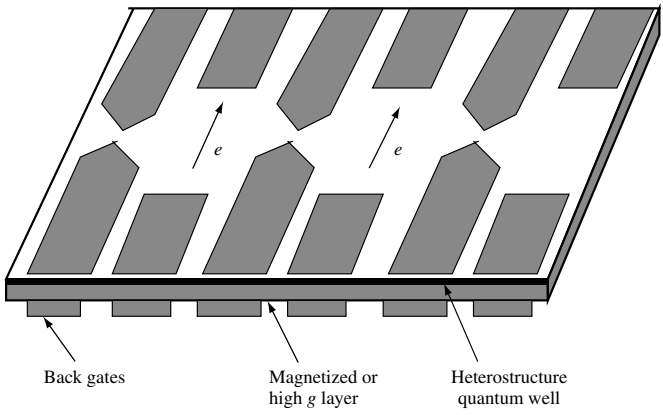

Figure 6.10 Schematic depiction of an array of quantum dots with electron spins as qubits. After Burkard *et al.* (2002).

we obtain the SWAP gate (6.37). It is easy to pass from a SWAP gate to a cNOT gate owing to the following identity (Exercise 4.6.4). One first obtains a cZ gate

$$\mathrm{cZ} = \mathrm{e}^{\mathrm{i}\pi\sigma_z^1/4}\,\mathrm{e}^{-\mathrm{i}\pi\sigma_z^2/4}\,U_{\mathrm{SWAP}}^{1/2}\,\mathrm{e}^{\mathrm{i}\pi\sigma_z^1/2}\,U_{\mathrm{SWAP}}^{1/2}, \tag{6.63}$$

where

$$U_{\mathrm{SWAP}}^{1/2} = \frac{1}{1+\mathrm{i}}\begin{pmatrix} 1+\mathrm{i} & 0 & 0 & 0 \\ 0 & 1 & \mathrm{i} & 0 \\ 0 & \mathrm{i} & 1 & 0 \\ 0 & 0 & 0 & 1+\mathrm{i} \end{pmatrix},$$

and (6.15) is used for going from a cZ gate to a cNOT gate. The coupling $J(t)$ can be switched on and off by raising and lowering the tunnel barrier between the two dots (Fig. 6.10). In GaAs semiconductors the main source of decoherence comes from the hyperfine coupling to the nuclear spins, as both Ga and As possess a nuclear spin $I = 3/2$. Another source of decoherence is due to the external leads needed for readout.

6.5 Exercises

6.5.1 Off-resonance Rabi oscillations

Starting from the Hamiltonian (6.4) in the rotating reference frame, show that $\exp(-\mathrm{i}\tilde{H}t)$ can be written as

$$\exp(-\mathrm{i}\tilde{H}t/\hbar) = \exp\left[-\frac{\mathrm{i}\Omega t}{2}\left(\frac{\delta}{\Omega}\,\sigma_z - \frac{\omega_1}{\Omega}\,\sigma_x\right)\right]$$

with $\Omega = \sqrt{\delta^2 + \omega_1^2}$. The vector

$$\hat{n} = \left(n_x = -\frac{\omega_1}{\Omega}, n_y = 0, n_z = \frac{\delta}{\Omega} \right)$$

is a unit vector. Show that

$$\exp(-\mathrm{i}\tilde{H}t/\hbar) = \left(\cos\frac{\Omega t}{2} - \mathrm{i}\frac{\delta}{\Omega}\sin\frac{\Omega t}{2} \right) |0\rangle\langle 0| + \mathrm{i}\frac{\omega_1}{\Omega}\sin\frac{\Omega t}{2}\left(|0\rangle\langle 1| + |1\rangle\langle 0|\right) + \left(\cos\frac{\Omega t}{2} + \mathrm{i}\frac{\delta}{\Omega}\sin\frac{\Omega t}{2} \right) |1\rangle\langle 1|.$$

6.5.2 Commutation relations between the a and $a^\dagger$

1. Use (6.19) and (6.21) to prove the commutation relation $[a, a^\dagger] = I$.
2. Calculate the commutator $[a^\dagger a, a]$. From this derive the second line of (6.30).

6.5.3 Construction of a cZ gate using trapped ions

1. Let us consider the case of a single trapped ion. The laser field applied to the ion has the form (6.27) for $t > 0$. We work in the reference frame rotating at frequency ω_0 (and not ω as in the case of NMR), where the interaction Hamiltonian $\tilde{H}_{\mathrm{int}}(t)$ is given by

$$\tilde{H}_{\mathrm{int}}(t) = \mathrm{e}^{\mathrm{i}\hat{H}_0 t/\hbar}\,\hat{H}_{\mathrm{int}}(t)\,\mathrm{e}^{\mathrm{i}\hat{H}_0 t/\hbar}.$$

Show that the rotating-wave approximation leads to the Hamiltonian

$$\tilde{H}_{\mathrm{int}} \simeq -\frac{\hbar}{2}\omega_1\left[\sigma_+\,\mathrm{e}^{\mathrm{i}(\delta t-\phi)}\,\mathrm{e}^{-\mathrm{i}kz} + \sigma_-\,\mathrm{e}^{-\mathrm{i}(\delta t-\phi)}\,\mathrm{e}^{\mathrm{i}kz}\right],$$

where $\delta = \omega - \omega_0$ is the detuning. If $\delta = 0$, this Hamiltonian is independent of time:

$$\tilde{H}_1 \simeq -\frac{\hbar}{2}\omega_1\left[\sigma_+\,\mathrm{e}^{-\mathrm{i}\phi}\,\mathrm{e}^{-\mathrm{i}kz} + \sigma_-\,\mathrm{e}^{\mathrm{i}\phi}\,\mathrm{e}^{\mathrm{i}kz}\right].$$

2. Let m and $m + m'$ be two levels of the harmonic oscillator. Show that the Rabi frequency $\omega_1^{m\to m+m'}$ is given by

$$\omega_1^{m\to m+m'} = \omega_1 |\langle m + m'|\mathrm{e}^{\mathrm{i}\eta(a+a^\dagger)}|m\rangle|,$$

where η is the Lamb–Dicke parameter. In particular, show that in the Lamb–Dicke approximation $\eta \ll 1$, and for $m' = \pm 1$ we have the following for the blue and red side-bands (see Fig. 6.4):

$$\omega_1^{m\to m+1} \simeq \eta\sqrt{m+1}\,\omega_1 = \omega_1^+ \quad \text{(blue)},$$
$$\omega_1^{m\to m-1} \simeq \eta\sqrt{m}\,\omega_1 = \omega_1^- \quad \text{(red)}.$$

Derive the Hamiltonian for the two bands, first for the blue side-band

$$\tilde{H}^{+}_{\text{int}} = \frac{\mathrm{i}}{2}\,\eta\,\hbar\omega_1\sqrt{m+1}\left[\sigma_+ a_b\,\mathrm{e}^{-\mathrm{i}\phi} - \sigma_- a_b^\dagger\,\mathrm{e}^{\mathrm{i}\phi}\right],$$

and then for the red side-band

$$\tilde{H}^{-}_{\text{int}} = \frac{\mathrm{i}}{2}\,\eta\,\hbar\omega_1\sqrt{m}\left[\sigma_+ a_r^\dagger\,\mathrm{e}^{-\mathrm{i}\phi} - \sigma_- a_r\,\mathrm{e}^{\mathrm{i}\phi}\right].$$

The operators $a_b \cdots a_r^\dagger$ are defined so as to preserve the norm of the state vectors:

$$a_b = \frac{a}{\sqrt{m+1}}, \qquad a_b^\dagger = \frac{a^\dagger}{\sqrt{m+1}}, \qquad a_r = \frac{a}{\sqrt{m}}, \qquad a_r^\dagger = \frac{a^\dagger}{\sqrt{m}}.$$

We limit ourselves to the case $m = 1$. What are the rotation operators on the two bands $R^{\pm}(\theta, \phi)$, where $\theta = -\omega_1^{\pm} t$? $R^{\pm}(\theta, \phi)$ is a rotation by an angle θ about an axis in the xOy plane making an angle ϕ with the axis Ox and using the blue $(+)$ or red $(-)$ side-band.

3. In addition to the levels $|0, 0\rangle$, $|0, 1\rangle$, $|1, 0\rangle$, and $|1, 1\rangle$ of Fig. 6.3(a), we also use the level $|1, 2\rangle$. Sketch the level scheme and identify the transitions of the blue side-band $|0, 0\rangle \leftrightarrow |1, 1\rangle$ and $|0, 1\rangle \leftrightarrow |1, 2\rangle$. Show that the rotation operator $R^{+}_{\alpha\beta}$, defined as

$$R^{+}_{\alpha\beta} = R^{+}(\alpha, \pi/2)\, R^{+}(\beta, 0)\, R^{+}(\alpha, \pi/2)\, R^{+}(\beta, 0),$$

is equal to $-I$ for $\alpha = \pi$ and any β or for $\beta = \pi$ and any α. Using the fact that the Rabi frequency for the transition $|0, 1\rangle \leftrightarrow |1, 2\rangle$ is $\sqrt{2}$ times that for the transition $|0, 0\rangle \leftrightarrow |1, 1\rangle$, how can α and β be chosen such that $R^{+}_{\alpha\beta} = -I$ for the two transitions? Find the sequence of 4 pulses and their duration such that the net result is

$$|00\rangle \leftrightarrow -|0, 0\rangle, \qquad |0, 1\rangle \leftrightarrow -|0, 1\rangle, \qquad |1, 0\rangle \leftrightarrow +|1, 0\rangle, \qquad |1, 1\rangle \leftrightarrow -|1, 1\rangle.$$

This is how a cZ gate is constructed (up to a sign).

4. Now we need to "transfer" the cZ gate to the computational basis of the states $|n_1, n_2\rangle$, $n_1, n_2 = 0, 1$ being the ground and excited states of the two ions. Show that the desired result is obtained by sandwiching the rotation operator $R^{+(1)}_{\alpha\beta}$ on ion number 1 using the blue side-band between two π rotations on ion number 2 using the red side-band:

$$\left[R^{-(2)}(\pi, \pi/2)\right] R^{+(1)}_{\alpha\beta} \left[R^{-(2)}(-\pi, \pi/2)\right].$$

Using (6.15), one goes from a cZ gate to a cNOT gate, but a slightly more complicated operation allows the direct construction of a cNOT gate.

https://doi.org/10.1017/CBO9780511755361.008

6.5.4 Vibrational normal modes of two ions in a trap

The potential energy of the two ions is

$$V = \frac{1}{2} M\omega_z^2 \left(z_1^2 + z_2^2\right) + \frac{q^2}{4\pi\varepsilon_0} \frac{1}{|z_1 - z_2|}.$$

Find the equilibrium positions of the two ions. Show that the vibrational eigenfrequencies are ω_z and $\sqrt{3}\omega_z$. How can the vibrational amplitudes of these two normal modes be characterized? Hint: the equilibrium positions being $\pm z_0$, write $z_1 = z_0 + u$, $z_2 = -z_0 + v$, and expand V to second order in (u, v).

6.5.5 Meissner effect and flux quantization

1. Starting from (6.43) and using the Maxwell equation $\vec{\nabla} \times \vec{B} = \mu_0 \vec{j}_{\text{em}}$, show that the magnetic field $\vec{B}$ obeys

$$\nabla^2 \vec{B} = \frac{1}{\lambda_{\text{L}}^2} \vec{B},$$

where λ_{L} is the London penetration length. Give the expression for λ_{L}. Assume a one-dimensional geometry, where the region $z < 0$ is normal while the region $z > 0$ is superconducting. Show that $\vec{B}$ and, consequently, $\vec{j}_{\text{em}}$ decrease as $\exp(-z/\lambda_{\text{L}})$. The electromagnetic current and the magnetic fields are therefore excluded from the bulk of the superconducting region.

2. Consider a contour C drawn in the bulk of a superconducting ring. Using $\vec{j}_{\text{em}} = 0$ along C, derive (6.44) and (6.52).

6.5.6 Josephson current

By separating the real and imaginary parts in the equations (6.45) for ψ_1 and ψ_2, show that

$$\frac{\mathrm{d}\rho_1}{\mathrm{d}t} = \frac{2K}{\hbar}(\rho_1\rho_2)^{1/2} \sin\theta,$$

$$\frac{\mathrm{d}\rho_2}{\mathrm{d}t} = -\frac{2K}{\hbar}(\rho_1\rho_2)^{1/2} \sin\theta,$$

$$\frac{\mathrm{d}\theta_1}{\mathrm{d}t} = -\frac{K}{\hbar}\left(\frac{\rho_2}{\rho_1}\right)^{1/2} \cos\theta - \frac{q_{\text{C}}V}{2\hbar},$$

$$\frac{\mathrm{d}\theta_2}{\mathrm{d}t} = \frac{K}{\hbar}\left(\frac{\rho_1}{\rho_2}\right)^{1/2} \cos\theta + \frac{q_{\text{C}}V}{2\hbar}.$$

https://doi.org/10.1017/CBO9780511755361.008

Assuming that $\rho_1 \simeq \rho_2 = \rho$, deduce from these equations the Josephson current I_J:

$$I_J = \frac{d\rho_1}{dt} = -\frac{K\rho}{\hbar} \sin\theta = I_0 \sin\theta$$

and

$$\frac{d\theta}{dt} = \frac{q_C V}{\hbar}.$$

6.5.7 Charge qubits

The circuit is drawn in Fig. 6.11. The superconducting box (Cooper pair box) is divided into two parts by a Josephson junction. If C_J and C_g denote the capacitances of the junction and the external capacitor, respectively, and V_g is the applied voltage bias, the electrical energy stored in the circuit reads

$$E = E_c(n - n_g)^2 - E_J \cos\theta,$$

where θ is the junction phase difference. The energy E_c,

$$E_c = \frac{q_C^2}{2(C_J + C_g)},$$

is the electrostatic energy of the capacitors and $n (n \in \mathbb{Z})$ is the number of *excess* Cooper pairs in the right-hand box. Let N be the operator which counts the number of *excess* Cooper pairs in the right-hand box, with eigenstates $|n\rangle$, $N|n\rangle = n|n\rangle$, and let Θ be the conjugate operator, $[N, \Theta] = iI$. The eigenstates of Θ are denoted $|\theta\rangle$, $\Theta|\theta\rangle = \theta|\theta\rangle$, $0 \le \theta < 2\pi$.

1. Show that if we choose the scalar product $\langle n|\theta\rangle = \exp(-in\theta)$ such that

$$|\theta\rangle = \sum_{n=-\infty}^{+\infty} e^{-in\theta} |n\rangle,$$

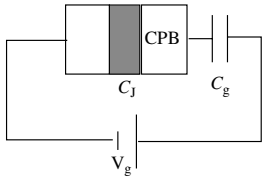

Figure 6.11 Superconducting circuit for charge qubits. CPB, Cooper pair box.

https://doi.org/10.1017/CBO9780511755361.008

then $N = \mathrm{i}\partial/\partial\theta$ and the commutation relation $[N, \Theta] = \mathrm{i}$ is satisfied. Note that the bases $\{|n\rangle\}$ and $\{\theta\rangle\}$ are complementary according to the definition of Section 2.4. Derive the completeness relation

$$\int_0^{2\pi} \frac{\mathrm{d}\theta}{2\pi} |\theta\rangle\langle\theta| = I$$

and deduce from this relation that

$$\cos\Theta = \frac{1}{2} \sum_{n=-\infty}^{+\infty} (|n\rangle\langle n+1| + |n+1\rangle\langle n|) .$$

2. In the $\{|n\rangle\}$ basis the quantum Hamiltonian reads

$$\hat{H} = E_\mathrm{c} \sum_{n=-\infty}^{+\infty} (n - n_\mathrm{g})^2 |n\rangle\langle n| - \frac{1}{2} E_\mathrm{J} \sum_{n=-\infty}^{+\infty} (|n\rangle\langle n+1| + |n+1\rangle\langle n|) .$$

We assume that $E_\mathrm{J} \ll E_\mathrm{c}$, so that the first term in $\hat{H}$ is dominant except when $n_\mathrm{g} \simeq p + 1/2$ with p an integer, in which case the first term gives the same energy $E_\mathrm{c}/4$ for the states $n = p$ and $n = p+1$. In the absence of the second term the two states would be exactly degenerate for $n_\mathrm{g} = p + 1/2$. For definiteness let us choose $n_\mathrm{g} = 1/2$. Show that in the vicinity of $n_\mathrm{g} = 1/2$ we can write

$$\hat{H} = -\frac{1}{2} B_z \sigma_z - \frac{1}{2} B_x \sigma_x ,$$

where $B_x = 0$ if $n_\mathrm{g} = 1/2$. Determine B_z and B_x as functions of the parameters in $\hat{H}$. Draw the level scheme at fixed B_x as a function of B_z, discuss the phenomenon of level repulsion, and show that the level scheme is similar to that of Fig. 6.9.

6.6 Further reading

The criteria for a quantum computer have been stated by di Vincenzo (2000). The concrete realizations of quantum computers are described by Nielsen and Chuang (2000), Chapter 7, by Bouwmeester *et al.* (2000) and by Stolze and Suter (2004), Chapters 9 to 12. The experimentally performed (NMR) factorization of 15 using the Shor algorithm was realized by Vandersypen *et al.* (2001); see also Vandersypen and Chuang (2004). The article by Cirac and Zoller (2004) describes recent results on trapped ions and Bose–Einstein condensates, and that of Mooij (2004) describes the results obtained using Josephson junctions; see also You and Nori (2005). Another useful review on trapped ions is Leibfried *et al.* (2003). The standard results on the quantum harmonic oscillator can be found in any quantum mechanics textbook, for example, Le Bellac (2006), Chapter 11; Doppler cooling

is described in Section 14.4 of the same book. A complete panorama of the recent developments in quantum information theory is given at an advanced level in the proceedings of the Les Houches School 2003; see, in particular, the courses of Jones (2004), Blatt (2004), and Devoret and Martinis (2004). The use of quantum dots is described by Burkard *et al.* (2002).

https://doi.org/10.1017/CBO9780511755361.008